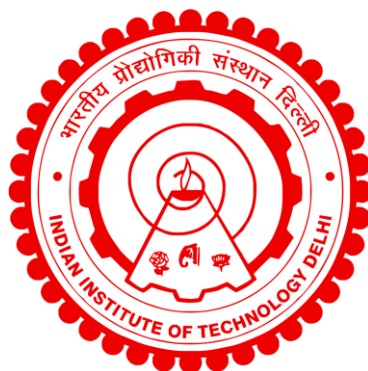


**CONVERSION OF LIGHT CYCLE OIL TO BENZENE AND
ALKYLATED MONOAROMATICS OVER VARIOUS
MONOMETALLIC AND BIMETALLIC OXIDE CATALYSTS
IN THE PRESENCE OF HYDROGEN DONOR**

AKSHATA RAMTEKE



**DEPARTMENT OF CHEMICAL ENGINEERING
INDIAN INSTITUTE OF TECHNOLOGY DELHI
JANUARY 2025**

© Indian Institute of Technology Delhi (IITD), New Delhi, 2025

**Conversion of light cycle oil to benzene and alkylated mono-
aromatics over various monometallic and bimetallic oxide
catalysts in the presence of hydrogen donor**

by

Akshata Ramteke

Department of Chemical Engineering

Submitted

In fulfillment of the requirements of the degree of

Doctor of Philosophy

to the



Indian Institute of Technology Delhi

January 2025

Dedicated to my Parents

Savita Ramteke and Vijay Ramteke

Without whom this Ph.D. journey would have been incomplete

Certificate

This is to certify that the thesis entitled “**Conversion of light cycle oil to benzene and alkylated mono-aromatics over various monometallic and bimetallic oxide catalysts in the presence of hydrogen donor**” being submitted by **Ms. Akshata Ramteke** to the Indian Institute of Technology Delhi for the award of the degree of **Doctor of Philosophy** is a record of *bonafide* research work carried out by her. **Ms. Akshata Ramteke** has worked under our guidance and supervision and has fulfilled the requirements for the submission of this thesis, which to our knowledge has reached the requisite standard. The research report and results presented in this thesis are original and have not been submitted, in part or full, to any other University or Institute for the award of any other degree or diploma.

Dr. K. K. Pant

Professor,

Department of Chemical Engineering

Indian Institute of Technology Delhi

New Delhi-110016

Dr. Divesh Bhatia

Professor,

Department of Chemical Engineering

Indian Institute of Technology Delhi

New Delhi-110016

Acknowledgments

Every project combines the knowledge and experience of both students and experts, with proper guidance being essential. I express my profound gratitude to **Prof. Divesh Bhatia** and **Prof. K.K. Pant** from the Department of Chemical Engineering at IIT Delhi, whose mentorship made this project possible. Their invaluable guidance, encouragement, and constructive criticism over the past six years have been instrumental in my research. Despite their busy schedules, they reviewed my work and provided crucial feedback, greatly enhancing its quality. Working under their esteemed guidance has been an unforgettable experience, and their kindness and support are deeply appreciated. I am also thankful to the Head of the Department of Chemical Engineering Indian Institute of Technology Delhi and all the faculty members of the department for their support and valuable suggestions. I wish to convey my gratitude to members of my research committee Prof. M. Ali Haider, Prof. S. Upadhyayula, and Prof. Nidhi Jain for their valuable suggestions and critical review of my work. I am thankful to all the staff members in the departmental characterization laboratory and Central Research Facility (CRF), their eagerness to help will always be appreciated and remembered.

I express my special thanks to my senior lab members Dr. Sonal Asthana, Dr. Rohit Kumar, Dr. Sourabh Mishra, Dr. Uma Dwivedi, Dr. Ejaz Ahmed, Dr. Sonit Balyan, Dr. Kaushal Parmar, Dr. Prashant Jadhao, Dr. Ashish Bohre, Dr. Kunwar Pal, Dr. Arindam Modak, Dr. Akshay Mankar, Dr. Rajan Singh, Dr. Ramdayal Panda, Dr. Komal Tripathi, and Dr. Sagar Dhanuskar, for their valuable suggestions to make the research work more cordial. I would like to thank my colleagues in the lab Dr. Shreya Singh, Dr. Amrita Preetam, Dr. Snigdha Mishra, Dr. Vaibhav Pandey, Dr. Vallari Chourasia, Dr. S.C Tiwari, Mr. Pranit Samanta, Mr. Venkanna, Mr. Shashank Shekhar Pandey, Ms. Iqra, Dr. Deepti Mishra, Ms. Komal Sharma, Mr. Avijit Das, Dr. Marut Jain, Dr. Sadaf, Ms. Shally Gupta, Mr. Abhishek Shao, Ms. Nidhi Kushwaha, Mr. Abdul, Ms. Neetu, Ms. Aisha Noor, Mr. Kaushik Kundu, Ms. Marvi Kaushik,

Dr. Pranav kherdekar, Ms. Chaitra Borkar, Mr. Ilyas Yusuf Mir, and Mr. Vishal Yogi for the peasant lab environment and for helping me with doubts throughout my studies. I am thankful to all my friends of IIT Delhi Mr. Manoj Kumar Beriya, and Mr. Ranjan Singh. I would like to thank Dr. Omvir Singh and my M. Tech senior Dr. Payal Bhautik for fruitful technical discussion during my Ph.D. I would like to extend my thanks to Mr. Vishesh Kumar, Mr. Krishna Kumar, Mr. Suchit Kumar, Mr. Ashish, and Mr. Vijay Pal for their constant help in every possible way to carry forward my research and performing experiments.

I have no words to express the motivation and inspiration given by my parents Mr. Vijay Ramteke and Mrs. Savita Ramteke, whose courage through their life has been a spiritual inspiration to me and holds no bounds. Their encouraging words and deeds through these tough and emotional times will always remain in my heart and soul. I am thankful to my sister (Poonam) and brother (Aman Ramteke) for their constant moral support and motivation during my studies. I cannot thank enough my whole family for having faith and trust in all my dreams and allowing me to pursue my goals without any bindings. I am also grateful to my bestfriend Dr. Nikhil Dhimole for his encouragement, support, and care throughout my research work. I am deeply grateful to my beloved pets Summu and Duggu, whose love and companionship bring immense joy to my life. A special thanks to Jimmy, the cherished dog from the IIT Delhi campus, who holds a special place in my heart. They have been my source of happiness and balance throughout this journey. I also want to express my sincere thanks to all those who had directly or indirectly helped me at various stages of this work thereby making it a total success. At last, thanks to the almighty God for his blessing and for giving me patience, strength, and peace throughout the journey of life.

Akshata Ramteke

Abstract

The per capita consumption of polymers is projected to increase, while the demand for conventional fuels like gasoline and diesel is expected to decrease. This shift has prompted a focus on converting crude to chemicals. Light cycle oil (LCO), with high amounts of sulfur and aromatics, has a low cetane number, making it unsuitable for diesel blends. Converting LCO to benzene, toluene, and xylene (BTX) can meet the rising chemical demand and utilize low-quality LCO feedstock. However, LCO conversion under FCC conditions is typically low, necessitating modifications to catalysts and processes for higher BTX yields. Even though various studies have been performed on bifunctional monometallic and bimetallic oxide catalysts at high pressure, their application at atmospheric pressure has not yet been studied. In this study, the selective conversion of diaromatics and triaromatics in LCO into monoaromatics using bifunctional catalysts is studied under FCC conditions. The hydrogen donor source utilized was n-hexadecane (n-HD) at atmospheric pressure instead of H₂. Thermodynamic analysis and cracking experiments indicate that the optimal temperature for maximizing BTX yield is 550 °C. n-HD is found to be an effective hydrogen donor when co-fed with LCO, resulting in enhanced BTX yield and reduced coke formation, with a 30 wt. % concentration shown to optimize feed conversion. Catalytic cracking experiments highlight Beta zeolite's superior activity compared to other zeolites (Y, ZSM-5, and Mordenite), and the trends are correlated to the acidity and structural characteristics such as pore volume, pore diameter, crystallite size, and surface area. Additionally, DFT calculations show that amongst various zeolites, Beta zeolite exhibits the lowest activation barrier for 1-methylnaphthalene cracking. The distinct reactivity levels of triaromatic, diaromatic, and condensed polyaromatic compounds are highlighted, with triaromatic compounds exhibiting the highest reactivity. These results are explained by the degree of unsaturation and bond angle analysis. Both monometallic (Ni, W, Co, Mo) and bimetallic (NiW, CoMo) oxide catalysts supported on

various zeolites (Mordenite, ZSM-5, Beta, Y, and Mix) were investigated. Bimetallic oxide catalysts exhibited superior performance, displaying higher total monoaromatic hydrocarbon (MAH) yield, BTX yield, and feed conversion compared to monometallic oxide catalysts. This improvement was attributed to the formation of bimetallic oxide species along with their strong interactions with the support, as evidenced by XPS, H₂-TPR, and UV-DRS analyses. Bimetallic oxide catalysts also demonstrated higher moderate acidity, an optimal balance of Brønsted and Lewis acid sites, and a higher hydrogen transfer index, explaining their higher BTX yield and lower coke formation. Experiments with n-HD as the sole reactant indicated that LCO primarily contributed to MAH formation, with n-HD serving as the hydrogen source. DFT simulations aligned with experimental findings, showing that bimetallic oxide catalyst had the lowest activation barrier for 1MN cracking in the presence of n-HD. The selective cracking of triaromatic compounds to diaromatics was rapid, with the conversion of diaromatics governing total MAH yield and the cracking of monoaromatic-2-ring compounds governing BTX production. An inverse correlation between the selectivity for 2-ring monoaromatics and BTX shows the formation of 2-ring monoaromatics as intermediates. Based on detailed product characterization, reaction pathways for the conversion of diaromatic and triaromatic are proposed. Additionally, a Co/Mo ratio above 0.5 leads to the formation of a dense CoMoO₄ phase, adversely affecting catalytic activity, while the optimal Co/Mo ratio of 0.5 maximizes BTX yields and minimizes coke production. Similar reactivity among alkylated naphthalene compounds suggested grouping them in developing a lumped kinetic model. A 12-lump kinetic model was developed based on the experimental data to elucidate the kinetic characteristics of LCO cracking on the CoMo/Beta catalyst, serving as a foundational tool for optimizing catalytic processes in refinery operations.

Keywords: Light cycle oil (LCO); BTX; Bifunctional catalysts; Hydrogen donor; Bimetallic catalysts; Structure-activity relation; FCC; Cracking

सार

पॉलिमर के प्रति व्यक्ति की खपत में वृद्धि की अपेक्षा है, जबकि पारंपरिक ईंधनों जैसे कि गैसोलीन और डीज़ल की मांग में कमी आने की संभावना है। इस बदलाव ने कच्चे तेल को रसायनों में परिवर्तित करने पर ध्यान केंद्रित करने के लिए प्रेरित किया है। लाइट सायकल तेल, जिसमें उच्च मात्रा में अरोमैटिक्स और सल्फर होता है, की सेटेन संख्या कम होती है, जिससे यह डीज़ल मिश्रण के लिए अनुपयुक्त हो जाता है। लाइट सायकल तेल को बेंजीन, टोल्युइन और ज़ाइलिन (बीटीएक्स) में परिवर्तित करना बढ़ती रासायनिक मांग को पूरा कर सकता है और निम्न गुणवत्ता वाले लाइट सायकल तेल फीडस्टॉक का उपयोग कर सकता है। हालांकि, एफसीसी स्थितियों के तहत लाइट सायकल तेल का रूपांतरण आमतौर पर कम होता है, जिससे बीटीएक्स की उपज बढ़ाने के लिए उत्प्रेरकों और प्रक्रियाओं में संशोधन की आवश्यकता होती है। जबकि विभिन्न अध्ययनों में उच्च दबाव पर बायफंक्शनल मोनोमेटलिक और बायमेटलिक ऑक्साइड उत्प्रेरकों का उपयोग किया गया है, उनकी वायुमंडलीय दबाव पर उपयोग का अभी तक अध्ययन नहीं किया गया है। इस अध्ययन में, एफसीसी स्थितियों के तहत बायफंक्शनल उत्प्रेरकों का उपयोग करके लाइट सायकल तेल में डायरोमैटिक्स और ट्राईरोमैटिक्स को मोनोरोमैटिक्स में परिवर्तित करने का अध्ययन किया गया है। हाइड्रोजन डोनर स्रोत के रूप में H_2 के बजाय न-हेक्साडेकेन का उपयोग किया गया। थर्मोडायनामिक विश्लेषण और क्रैकिंग प्रयोगों से पता चलता है कि बीटीएक्स की अधिकतम उपज के लिए सर्वोत्तम तापमान $550\text{ }^\circ\text{C}$ है। लाइट सायकल तेल के साथ सह-फीड के रूप में न-हेक्साडेकेन को उपयोग करने से बीटीएक्स की उपज में सुधार और कोक निर्माण में कमी होती है, जिसमें 30 wt. % की

सांद्रता फीड रूपांतरण के लिए अनुकूल होती है। कैटेलिटिक क्रैकिंग प्रयोगों से पता चला है कि बीटा ज़ियोलाइट का प्रदर्शन अन्य ज़ियोलाइट्स (वाई, जेडएसएम-5, और मोर्डेनाइट) की तुलना में बेहतर है, और प्रवृत्तियों को अम्लता और संरचनात्मक विशेषताओं (जैसे क्रिस्टलाइट का आकार, छिद्र का आयतन, छिद्र का व्यास, और सतह क्षेत्र) से जोड़ा गया है। इसके अलावा, डीएफटी गणनाएँ दिखाती हैं कि विभिन्न ज़ियोलाइट्स के बीच, बीटा ज़ियोलाइट का 1-मिथिलीनाफथालीन क्रैकिंग के लिए सबसे कम सक्रियता बाधा है। ट्रायरोमैटिक, डायरोमैटिक, और संकुचित पॉलीअरोमैटिक यौगिकों की भिन्न प्रतिक्रियाशीलता को उजागर किया गया है, जिसमें ट्रायरोमैटिक यौगिकों की उच्चतम प्रतिक्रियाशीलता होती है। ये परिणाम असंतृप्तता और बंध कोण विश्लेषण के माध्यम से समझाए गए हैं। मोनोमेटलिक (को, मो, नी, डब्ल्यू) और बायमेटलिक (कोमो, नी-डब्ल्यू, नीमो) ऑक्साइड उत्प्रेरकों का विभिन्न ज़ियोलाइट्स (मोर्डेनाइट, जेडएसएम-5, बीटा, वाई, और मिक्स) पर अध्ययन किया गया। बायमेटलिक ऑक्साइड उत्प्रेरकों ने उत्कृष्ट प्रदर्शन दिखाया, जिसमें मोनोमेटलिक ऑक्साइड उत्प्रेरकों की तुलना में उच्च कुल मोनोरोमैटिक हाइड्रोकार्बन (एमएएच) उपज, बीटीएक्स उपज, और फीड रूपांतरण पाया गया। इस सुधार को बायमेटलिक ऑक्साइड प्रजातियों के निर्माण और उनके समर्थन के साथ मजबूत अंतःक्रियाओं के लिए जिम्मेदार ठहराया गया है, जैसा कि H_2 -TPR, XPS, और UV-DRS विश्लेषणों से स्पष्ट हुआ है। बायमेटलिक ऑक्साइड उत्प्रेरकों ने उच्च मध्यम अम्लता, ब्रॉन्स्टेड और लुईस अम्ल साइट्स का अनुकूल संतुलन, और उच्च हाइड्रोजन ट्रांसफर इंडेक्स प्रदर्शित किया, जो उनकी उच्च बीटीएक्स उपज और कम कोक उत्पादन को स्पष्ट करता है। न-हेक्साडेकेन को एकमात्र अभिकर्ता के रूप में उपयोग करने पर, लाइट

सायकल तेल मुख्य रूप से मोनोरोमैटिक्स के निर्माण में योगदान करता है, जिसमें न-हेक्साडेकेन हाइड्रोजन स्रोत के रूप में कार्य करता है। डीएफटी सिमुलेशंस ने प्रयोगात्मक निष्कर्षों के साथ संरेखित किया, दिखाते हुए कि बायमेटलिक ऑक्साइड उत्प्रेरकों का न-हेक्साडेकेन की उपस्थिति में 1-एमएन क्रैकिंग के लिए सबसे कम सक्रियता बाधा है। ट्रायरोमैटिक यौगिकों का डायरोमैटिक में चयनात्मक क्रैकिंग तेजी से होती है, जिसमें डायरोमैटिक्स का रूपांतरण कुल मोनोरोमैटिक उत्पादन को नियंत्रित करता है और 2-रिंग मोनोरोमैटिक यौगिकों का क्रैकिंग बीटीएक्स उत्पादन को प्रभावित करता है। 2-रिंग मोनोरोमैटिक्स के लिए चयनता और बीटीएक्स के बीच एक विपरीत संबंध दर्शाता है, जिसमें 2-रिंग मोनोरोमैटिक्स मध्यवर्ती के रूप में कार्य करता है। उत्पाद वितरण के विश्लेषण ने डायरोमैटिक और ट्रायरोमैटिक क्रैकिंग के लिए एक तंत्र का प्रस्तावित किया। इसके अलावा, को/मो का अनुपात 0.5 से अधिक होने पर घन कोमोओ₄ चरण का निर्माण होता है, जो कैटेलिटिक गतिविधि को नकारात्मक रूप से प्रभावित करता है, जबकि 0.5 का आदर्श को/मो अनुपात बीटीएक्स उपज को अधिकतम करता है और कोक उत्पादन को न्यूनतम करता है। अल्काइलित नाफथालीन यौगिकों के बीच समान प्रतिक्रियाशीलता ने सुझाव दिया कि उन्हें एक समूह में विकसित किया जाए ताकि एक लंपड काइनेटिक मॉडल विकसित किया जा सके। प्रयोगात्मक डेटा के आधार पर 12-लंप काइनेटिक मॉडल विकसित किया गया है, जो कोमो/बीटा उत्प्रेरक पर लाइट सायकल तेल क्रैकिंग की काइनेटिक विशेषताओं को स्पष्ट करता है, जो रिफाइनरी संचालन में उत्प्रेरक प्रक्रियाओं के अनुकूलन के लिए एक मौलिक उपकरण के रूप में कार्य करता है।

Declaration by author

This thesis is composed of my original work and contains no material previously published or written by another person except where due reference has been made in the text. I have clearly stated the contribution of others to jointly authored works that I have included in my thesis.

I have clearly stated the contribution of others to my thesis as a whole, including statistical assistance, survey design, data analysis, significant technical procedures, professional editorial advice, financial support, and any other original research work used or reported in my thesis.

The content of my thesis is the result of work I have carried out since the commencement of my higher degree by research candidature and does not include a substantial part of work that has been submitted to qualify for the award of any other degree or diploma in any university or other tertiary institution. I have clearly stated which parts of my thesis, if any, have been submitted to qualify for another award.

I acknowledge that an electronic copy of my thesis must be lodged with the University Library and, subject to the policy and procedures of the Indian Institute of Technology Delhi, the thesis be made available for research and study following the Copyright Act 1968 unless a period of embargo has been approved by the Dean of the Graduate School.

I acknowledge that the copyright of all material contained in my thesis resides with the copyright holder(s) of that material. Where appropriate I have obtained copyright permission from the copyright holder to reproduce material in this thesis and have sought permission from co-authors for any jointly authored works included in the thesis.

Publications included in this thesis

[1] Ramteke, A. V., Kaushik, M., Bhatia, D., & Pant, K. K. (2024). Effect of temperature, hydrogen donor, and zeolites on light cycle oil cracking: Thermodynamic, experimental, and DFT analyses. *Sustainable Energy & Fuels*, 8(16), 3740-3752. (Incorporated within Chapter 4).

[2] Ramteke, A. V., Bhatia, D., & Pant, K. K. (2024). Selective cracking of light cycle oil to monoaromatics over non-noble bifunctional zeolite-supported Ni and NiW catalysts. *Fuel*, 358, 130085. (Incorporated within Chapter 5).

[3] Ramteke, A. V., Bhatia, D., & Pant, K. K. (2023). Conversion of light cycle oil to benzene and alkylated monoaromatics over monometallic and bimetallic CoMo catalysts in the presence of hydrogen donor. *Fuel*, 342, 127737. (Incorporated within Chapter 6).

[4] Ramteke, A. V., Mishra, D., Mishra, S., Pant, K. K., & Bhatia, D. (2023). Conversion of fly-ash into pristine ZSM-5 and its application for methane dehydroaromatization reaction. *Journal of Industrial and Engineering Chemistry*. (Incorporated a few parts within Chapter 4).

Submitted manuscripts included in this thesis

I have no other manuscripts from the thesis submitted and under review at the time of submission.

To be submitted manuscripts containing thesis work

[6] Ramteke, A. V., Kaushik, M., Bhatia, D., & Pant, K. K. Cracking of light cycle oil into BTX over bifunctional CoMo catalysts supported on Beta zeolite: Structure-activity relationship, optimizing Co and Mo ratio, DFT and kinetic study (Under preparation)

[7] Ramteke, A. V., Bhatia, D., & Pant, K. K. Conversion of Light Cycle Oil to BTX using various bifunctional catalysts supported on fly-ash derived zeolites (Under preparation)

Contributions by others to the thesis

In the above-listed publications, my contribution to the authored works is specified by the order of author names. For papers included in this thesis, where I appeared as a first author, I was accountable for material synthesis, testing, experiments design and implementation, data analysis, drafting of the manuscript, and preparation of figures and tables. In paper 4, Ms. Marvi Kaushik provided me the theoretical insights by conducting DFT studies. For other sections of the papers, the corresponding authors Prof. K. K. Pant, and Prof. Divesh Bhatia guided conception and manuscript drafting. Prof. K. K. Pant was responsible for securing research funds that supported experimental consumables and measuring instruments.

Other publications during candidature

[1] Singh, O[#]., Ramteke, A. V[#]., Joshi, B., Vempatapu, B. P., Pant, K. K., Ray, A., & Sarkar, B. (2023). Sustainable Bioaromatics from Sapium Oil over Encaged AlPO₄ Zeolite Material: A Feasibility Study. *ACS Sustainable Chemistry & Engineering*, 11(48), 17061-17074.

[2] Sagar Dhanuskar, **Akshata Vijay Ramteke**, Yashi Agrawal, Ejaz Ahmad, Arindam Modak, K. K. Pant, Catalytic cracking and deoxygenation of cottonseed oil to produce light olefins over lanthanum impregnated zeolite. *Biomass and Bioenergy* (under review).

[2] Sagar Dhanuskar[#], **Akshata Vijay Ramteke**[#], Arindam Modak, K. K. Pant, Catalytic cracking and deoxygenation of cottonseed oil to produce light olefins over metal impregnated coal fly-ash derived ZSM-5. *Journal of Environmental Chemical Engineering* (under review).

Statement of parts of the thesis submitted to qualify for the award of another degree.

No works submitted towards another degree have been included in this thesis.

Research involving human or animal subjects.

No animal or human subjects were involved in this research.

Nomenclature

A_C	Area of the catalyst bed, m ²
A_T	total acidity (mmol/g)
C_R	relative crystallinity (%)
d_c	average crystallite size (nm)
D_{po}	average pore diameter (Å)
E_a	activation barrier (kJ/mol)
E_i	activation energy for the formation of species 'i' (kJ/mol)
F	objective function
k_{i_0}	pre-exponential factor for the formation of lump 'i' (1/sec)
k_i	kinetic constant for the formation of lump 'i' (m/sec)
M	mass of catalyst (g)
\dot{m}	mass flow rate of the feed (g/sec)
m_1	mass transfer coefficients
S_i	selectivity of the product 'i' (%)
r_i	rate of reaction
S_{micro}	micropore area (m ² g ⁻¹)
V_{cat}	volume of the catalyst in m ³
V_{meso}	mesopore volume (cm ³ g ⁻¹)
V_{micro}	micropore volume (cm ³ g ⁻¹)
V_{total}	total volume (cm ³ g ⁻¹)
WHSV	weight hourly space velocity (h ⁻¹)
w_j^{feed}	mass of component j at the reactor inlet (g)
$w_j^{product}$	mass of component j at the reactor outlet (g)
w_{LCO}^{feed}	mass of the LCO cut in the feed (g)
$w_{LCO}^{product}$	mass of the LCO cut in the product (g)
W_T^{feed}	total mass of the feed at the reactor inlet (g)
$X_{e,ind}$	individual equilibrium conversion (%)
$X_{e,ov}$	overall equilibrium conversion (%)
X_j	conversion of component j (%)
X_{LCO}	LCO conversion (%)
$Y_{e,BTX}$	equilibrium yield of BTX (%)
Y_i	yield of the product 'i' (%)
Y_{iS}	yield of lump 'i' at the surface (%)
φ	deactivation function
ΔH_{rxn}	heat of reaction (kJ/mol)

Abbreviations

1MN	1-methylnaphthalene
2MA	2-methylanthracene
2MN	2-methylnaphthalene
3MA	3-methylanthracene
3MN	3-methylnaphthalene
4MA	4-methylanthracene
4MN	4-methylnaphthalene
9MA	9-methylanthracene
Anth	anthracene
B	benzene
BaA	benz[a]anthracene
BAS	brønsted acid sites
B.E.	binding energy
BTX	benzene, toluene, and xylene
BTEX	benzene, toluene, ethyl benzene, and xylene
B3LYP	becke 3 parameter hybrid functional
CLO	clarified oil
COM	commercial
COTC	crude oil to chemicals
Di-AR	diaromatics
DFT	density functional theory
EB	ethyl benzene
FBP	final boiling point
FCC	fluidized catalytic cracking
FID	flame ionization detector
GC–DHA	gas chromatography with detailed hydrocarbon analysis
GGA	generalized gradient approximation
HCK	hydrocracking
HCN	heavy cracked naphtha
HCO	heavy cycle oil
HDT	hydrotreatment
HTI	Hydrogen transfer index
HSD	high-speed diesel
HCK	hydrocracking
IBP	initial boiling point
LAS	lewis acid sites
LCN	light cracked naphtha

LCO	light cycle oil
MAH	monoaromatic hydrocarbons
MAT	micro activity testing
MEP	minimum energy path
MPhA	methylphenanthrene
n-HD	n-hexadecane
NEB	nudged Elastic Band method
PAHs	polyaromatic hydrocarbons
PBE	Perdew–Burke–Ernzerhof exchange correlation
PhA	phenanthrene
PFO	pyrolysis fuel oil
SAR	silica to alumina ratio
SimDist	simulated distillation
T	toluene
TBP	true boiling point
TCD	thermal conductivity detector
TS	transition state
VASP	Vienna ab initio simulation package
VGO	vacuum gas oil
X	Xylene

Table of Contents

Acknowledgments.....	IV
Abstract.....	VI
संर.....	VIII
Declaration by author.....	XI
Publications included in this thesis	XII
Contributions by others to the thesis.....	XIII
Nomenclature.....	XIV
Abbreviations.....	XV
Table of Contents.....	XVII
List of Figures.....	XXI
List of Tables	XXVIII
Chapter 1. Introduction.....	1
1.1 Background and Motivation.....	1
1.2. Evolution and Integration of Petroleum Refining and the Petrochemical Industry	3
1.3. Petrochemical Feedstock: Aromatics	5
1.4. Role of Catalytic Cracking in COTC Configurations	6
1.5. Upgrading Light Cycle Oil (LCO).....	7
1.6. Research Objectives and outline	10
1.7. Thesis Organization.....	11
Chapter 2. Literature review.....	12
2.1. Background	12
2.2. LCO upgradation processes	13
2.2.1. Hydroprocessing (HPS).....	13
2.2.2. Catalytic Reforming	15
2.2.3. Solvent Extraction	16
2.2.4. Utilization of LCO Processing Techniques	16
2.3. Effect of catalyst in hydrocracking of LCO and its model compounds to fuels	18
2.4. Effect of catalyst in hydrocracking of LCO and its model compounds to BTX.....	23
2.5. Cracking of LCO Under FCC Conditions.....	28
2.6. Hydrogen transfer Reactions.....	33
2.7. Theoretical Studies on Catalytic Cracking.....	35
2.8. Kinetic Modelling	38
2.9. Gaps and Motivation for the Present Work.....	42

2.10. Research Objectives	43
Chapter 3. Material and Methods	44
3.1. Experimental Methods	44
3.2. Materials.....	44
3.3. Catalyst synthesis	45
3.3.1. Synthesis of monometallic and bimetallic catalysts	45
3.4. Catalyst characterization	46
3.4.1. X-ray Diffraction	46
3.4.2. Nitrogen-physisorption.....	46
3.4.3. Field emission scanning electron microscopy (FE-SEM) & High-resolution transmission electron microscopy (HR-TEM)	47
3.4.4. Hydrogen Temperature Programmed Reduction.....	47
3.4.5. Microwave Plasma Atomic Emission Spectroscopy (MPAES).....	48
3.4.6. UV-Visible Diffuse reflectance spectra (UV-Vis DRS).....	48
3.4.7. Ammonia Temperature Programmed Desorption	48
3.4.8. Raman Spectroscopy	49
3.4.9. Fourier transform infrared (FT-IR) Spectroscopy	49
3.4.10. X-Ray Photoelectron Spectroscopy (XPS).....	49
3.4.11. Pyridine-FTIR analysis.....	49
3.5. Analysis of LCO.....	50
3.5.1. GC-MS analysis.....	50
3.5.2. GC-SimDist analysis	50
3.5.3. CHNS analysis.....	50
3.5.4. GC-DHA analysis.....	51
3.5.5. GC (TCD and FID) analysis	51
3.6. Catalyst performance evaluation.....	51
3.7. Thermodynamic analysis.....	55
3.8. Molecular simulations	55
Chapter 4. Effect of temperature, hydrogen donor, and zeolites: Thermodynamic, experimental, and DFT analyses.....	57
4.1. Introduction	57
4.2. Results and Discussion.....	59
4.2.1. Zeolites characterization.....	59
4.2.2. LCO properties	60
4.2.3. Effect of temperature	62

4.2.4. Effect of hydrogen donors	66
4.2.5. Catalyst activity results.....	75
4.2.6. Effect of catalyst composition	82
4.3. Conclusions	83
Chapter 5. Selective cracking of light cycle oil to monoaromatics over Ni and NiW catalysts	85
5.1. Introduction	85
5.2. Results and Discussion.....	85
5.2.1. Catalyst characterization.....	85
5.2.2. LCO properties	98
5.2.3. Catalytic activity.....	99
5.3. Conclusions	121
Chapter 6. Conversion of light cycle oil over monometallic and bimetallic CoMo catalysts.	123
6.1. Introduction	123
6.2. Results and Discussion.....	124
6.2.1. Catalyst characterization.....	124
6.2.2. LCO properties	134
6.2.3. Catalytic activity.....	135
6.3. Conclusions	163
Chapter 7. Cracking of light cycle oil into BTX over CoMo/Beta catalysts with various Co/Mo ratios	166
7.1. Introduction	166
7.2. Results and Discussion.....	166
7.2.1. Catalyst characterization.....	166
7.2.2. LCO properties	178
7.2.3. Catalytic activity.....	178
7.3. Conclusions	192
Chapter 8. Development of kinetic model.....	194
8.1 Introduction	194
8.2. Results and Discussion.....	194
8.2.1. Lumped kinetic modelling.....	194
8.3. Conclusions	198
Chapter 9. Conclusion and recommendations	199
References.....	204
Appendix.....	221

Appendix A	221
Appendix B	224
Appendix C	237
Appendix D	247
Annexure-I	254

List of Figures

Fig. 1.1. Breakdown of total fuel consumption by energy source and sector for 2017 [Source: World Energy Consumption [6]].	2
Fig. 1.2. Indian petrochemicals scenario [source: ICIS [8]].	3
Fig. 1.3. Integrated refinery and petrochemical scenario [8-11].	3
Fig. 1.4. Global BTX demand growth [source: straits research [11-15]].	5
Fig. 1.5. Challenges of LCO blending in diesel Pool.	8
Fig. 1.6. Conventional LCO conversion process.	8
Fig. 1.7. Cost-effective LCO conversion process.	10
Fig. 2.1. Typical process Flow diagram for HPS unit [42].	14
Fig. 2.2. Solvent extraction process for BTX aromatics [46,47].	16
Fig. 2.3. Global Utilization of LCO Upgradation Techniques [48-50].	17
Fig. 2.4. Reaction pathways for HDT and HCK of naphthalene [20,21].	18
Fig. 2.5. Reaction pathway for the cracking of 1,3-dialkyl naphthalene [8].	19
Fig. 2.6. Possible ring-opening followed by hydrocracking reaction [52-53].	20
Fig. 2.7. Effect of pressure on naphtha selectivity and HCK Conversion [56].	22
Fig. 2.8. Reaction pathway of LCO hydrocracking [57].	23
Fig. 2.9. Hydrocracking of naphthalene to BTX [20,21].	24
Fig. 2.10. Reaction pathways for the cracking naphthalene [32].	31
Fig. 2.11. Reaction mechanism proposed for cracking of 3-ring PAHs [28].	35
Fig. 2.12. The proposed kinetic scheme by Ebrahimi et al [104].	41
Fig. 3.1. Schematic of bimetallic catalyst synthesis process.	46
Fig. 3.2. Schematic of the reactor setup.	52
Fig. 3.3. Schematic of the hydrocracking reactor setup.	55
Fig. 4.1. LCO sample composition based on the number of carbon atoms per molecule.	62
Fig. 4.2. Temperature effect on (a) feed conversion, and (b) BTX yield for cracking of LCO model compounds.	63
Fig. 4.3. Temperature effect on (a) feed conversion, (b) BTX yield, (c) MAH yield, and (d) coke yield for thermal cracking of LCO and its model compounds. Equilibrium feed conversion and BTX yield are indicated by triangular markers.	65
Fig. 4.4. Temperature effect on individual conversions of 1MN and 9MA (Feed mixture: 50 wt. % 1MN + 50 wt. % 9MA)	65

Fig. 4.5. (a) BTX and coke yield, and (b) product distribution for thermal cracking of different hydrogen donors and LCO cracking in the co-presence of hydrogen donors.....	67
Fig. 4.6. Composition of the gaseous product for cracking of hydrogen donors and LCO cracking in co-presence of hydrogen donors.	68
Fig. 4.7. Effect of proportion of n-HD in the feed on (a) overall feed conversion, (b) individual feed conversion, and (c) BTX yield at equilibrium for cracking of LCO model compounds (T = 550 °C).....	70
Fig. 4.8. Equilibrium product composition for cracking of (a) 1MN, (b) 9MA, and (c) 1MN + 9MA with varying n-HD concentrations (T = 550 °C).....	70
Fig. 4.9. Effect of temperature on overall equilibrium conversion of feed containing varying proportions of n-HD and (a) 1MN, (b) 9MA, and (c) 1MN + 9MA.	71
Fig. 4.10. Effect of different hydrogen donor percentages and temperature on equilibrium BTX yield during cracking of (a) 1MN, (b) 9MA, and (c) 1MN + 9MA.....	71
Fig. 4.11. Effect of n-HD percentage on (a) overall feed conversion, (b) individual feed conversion, (c) BTX yield, (d) MAH yield, and (e) coke yield for thermal cracking of LCO and its model compounds (T = 550 °C). Equilibrium feed conversion and BTX yield are indicated by triangular markers.	73
Fig. 4.12. Product distribution for thermal cracking of LCO at varying n-HD concentrations.	73
Fig. 4.13. Composition of the gaseous product during LCO cracking for varying n-HD concentrations.	74
Fig. 4.14. Optimized structures of reactant (R), product (P), and transition state (TS) for the interaction of H ₂ with the closest C-atom of 1MN. Bond distances are in Å.	74
Fig. 4.15. Feed conversions and product yields for catalytic cracking of LCO over various zeolites.	75
Fig. 4.16. Correlation between (a) BTX yield and crystallite size, (b) coke yield and average pore diameter, (c) coke yield and BET surface area, and (d) coke yield and total/micro pore volume.....	77
Fig. 4.17. Optimized structures of reactant (R), product (P), and transition state (TS) for the interaction of BAS with the closest C-atom of 1MN in Beta zeolite. Bond distances are in Å.	78
Fig. 4.18. Performance parameters for catalytic cracking of LCO (a) at various temperatures over Beta zeolite, and (b) in the absence and presence of 30 wt. % n-HD (T = 550 °C).	79

Fig. 4.19. Effect of thermal and catalytic cracking of LCO and its model compounds on (a) feed conversion, (b) BTX yield, (c) MAH yield, and (d) coke yield. (T = 550 °C).	81
Fig. 4.20. Individual conversions for the cracking of feed mixtures containing (a) 1MN (50 and 9MA (both 50 wt. %), and (b) 1MN, 9MA, and BaA (all 33.33 wt. %).	82
Fig. 4.21. BTX and coke yields for LCO cracking over various monometallic and bimetallic	82
Fig. 5.1. XRD pattern of (a) Beta zeolite, Ni/Beta, and NiW/Beta, (b) Y zeolite, Ni/Y, and NiW/Y, (c) Mordenite, Ni/Mordenite, and NiW/Mordenite, and (d) Mix zeolite, Ni/Mix, and NiW/Mix catalysts.	86
Fig. 5.2. Correlation between crystallite size and (a) total acidity, (b) BET surface area, (c) average pore diameter, and (d) total pore volume.	87
Fig. 5.3. NH ₃ -TPD profiles of (a) Ni/Beta, Ni/Y, Ni/Mordenite, and Ni/Mix, and (b) NiW/Beta, NiW/Y, NiW/Mordenite, and NiW/Mix catalysts	89
Fig. 5.4. H ₂ -TPR profile of (a) Ni/Beta, Ni/Y, Ni/Mordenite, and Ni/Mix, and (b) NiW/Beta, NiW/Y, NiW/Mordenite, and NiW/Mix catalysts.	92
Fig. 5.5. FE-SEM micrographs of (a) Beta zeolite, (b) Ni/Beta, (c) W/Beta, and (d) NiW/Beta.	93
Fig. 5.6. HR-TEM micrographs of (a) Beta zeolite, (b, c) Ni/Beta, (d, e) W/Beta, and (f, g) NiW/Beta at different resolutions.	94
Fig. 5.7. XPS spectra of (a) W 4f for W/Beta and NiW/Beta, and (b) Ni 2p for Ni/Beta and NiW/Beta.	95
Fig. 5.8. Raman spectra of (a) Ni/Beta, Ni/Y, Ni/Mordenite, and Ni/Mix, and (b) NiW/Beta, NiW/Y, NiW/Mordenite, and NiW/Mix catalysts.	97
Fig. 5.9. UV-DRS spectra of (a) Ni/Beta, Ni/Y, Ni/Mordenite, and Ni/Mix, and (b) NiW/Beta, NiW/Y, NiW/Mordenite, and NiW/Mix catalysts.	98
Fig. 5.10. (a) 2MN conversion, (b) diaromatics conversion, (c, d) BTX yield, (e, f) total MAH yield, and (g, h) coke yield over various catalysts with 2MN with and without n-HD.	100
Fig. 5.11. Correlation between BTX yield and (a) crystallite size, (b) BET surface area, (c) average pore diameter, and (d) total pore volume, with 2MN in the feed.	101
Fig. 5.12. Correlation between (a) BTX yield and BAS/LAS ratio, (b) BTX yield and HTI, (c) BTX yield and moderate acid sites, (d) coke yield and BAS/LAS ratio, (e) coke yield and HTI, (f) coke yield and moderate acid sites.	103
Fig. 5.13. Product composition for the cracking of n-HD.	104
Fig. 5.14. Product distribution for cracking of (a) 2MN, and (b) 2MN + n-HD.	104

Fig. 5.15. Composition of the gaseous product for 2MN and 2MN + n-HD cracking over (a) Ni/Beta, and (b) NiW/Beta catalysts.....	105
Fig. 5.16. (a) BTX yield, (b) total MAH yield, (c) coke yield, and (d) 2MN conversion, with 2MN in the reactant mixture with and without n-HD.....	106
Fig. 5.17. (a) 2MN conversion, (b) 9MA conversion, (c) diaromatics conversion, (d) triaromatics conversion, (e, f) BTX yield, (g, h) total MAH yield, and (i, j) coke yield with 2MN + 9MA with and without n-HD.	109
Fig. 5.18. (a) LCO conversion, (b) diaromatics conversion, (c) triaromatics conversion, (d, e) BTX yield, (f, g) total MAH yield, and (h, i) coke yield with LCO in the feed with and without n-HD.	112
Fig. 5.19. Comparison of BTX yield, total MAH yield, and coke yield for different feeds over NiW/Beta catalyst.....	114
Fig. 5.20. (a) Correlation between the proportion of monoaromatics and diaromatics in the product, for cracking of LCO in the presence and absence of n-HD.....	114
Fig. 5.21. Conversion of different diaromatic compounds present in LCO (a) without n-HD in the reactant mixture, and (b) with n-HD in the reactant mixture.....	116
Fig. 5.22. LCO conversion in different experimental runs after multiple regeneration and reuse cycles over NiW/Beta.	117
Fig. 5.23. Effect of (a) temperature, and (b) WHSV on total MAH yield, BTX yield, coke yield, and LCO conversion for LCO + n-HD cracking on NiW/Beta.	118
Fig. 5.24. Selectivity versus LCO conversion at different temperatures over NiW/Beta catalysts for cracking of LCO + n-HD.	119
Fig. 5.25. Composition of the gaseous product for cracking of n-HD and LCO + n-HD over NiW/Beta.	119
Fig. 5.26. (a) XRD, (b) Raman, and (c) H ₂ -TPR analysis of fresh and used Ni/Beta and NiW/Beta catalysts.....	120
Fig. 6.1. XRD pattern of (a) Beta zeolite, Mo/Beta, Co/Beta, CoMo/Beta, and (b) Y zeolite, Mo/Y, Co/Y, CoMo/Y catalysts.	125
Fig. 6.2. NH ₃ -TPD profiles of (a) Beta zeolite, Mo/Beta, Co/Beta, CoMo/Beta, and (b) Y zeolite, Mo/Y, Co/Y, CoMo/Y catalysts.....	127
Fig. 6.3. H ₂ -TPR profile of (a) Mo/Beta, Co/Beta, CoMo/Beta, and (b) Mo/Y, Co/Y, CoMo/Y catalysts.....	129
Fig. 6.4. FE-SEM images of (a) Beta zeolite, (b) CoMo/Beta, (c) Y zeolite, and (d) CoMo/Y catalysts.....	129

Fig. 6.5. HR-TEM images of (a,b) Beta zeolite, (c,d) CoMo/Beta, (e,f) Y zeolite, and (g,h) CoMo/Y at different resolutions.	130
Fig. 6.6. XPS spectra of (a) Mo 3d for Mo/Beta, CoMo/Beta, (b) Mo 3d for Mo/Y, CoMo/Y, (c) Co 2p for Co/Beta, CoMo/Beta, and (d) Co 2p for Co/Y, CoMo/Y.	131
Fig. 6.7. Raman spectra of (a) Beta zeolite, Mo/Beta, Co/Beta, CoMo/Beta, and (b) Y zeolite, Mo/Y, Co/Y, CoMo/Y catalysts.	133
Fig. 6.8. UV-DRS spectra of (a) Mo/Beta, Co/Beta, CoMo/Beta, and (b) Mo/Y, Co/Y, CoMo/Y catalysts.	134
Fig. 6.9. Feed composition of LCO based on (a) type of compounds and (b) number of carbon atoms per molecule.	135
Fig. 6.10. Product distribution for 1MN and 1MN + n-HD cracking over (a) Beta zeolite and catalysts supported over Beta zeolite, (b) Y zeolite and catalysts supported over Y zeolite (Temperature - 500 °C, Pressure - 1 atm, WHSV - 83 h ⁻¹ , catalyst mass - 4 g, liquid feed injected - 3.7 g, feed - 1MN (in the absence of n-HD) or 70 wt. % 1MN + 30 wt. % n-HD).....	139
Fig. 6.11. Composition of the gaseous product for 1MN and 1MN + n-HD cracking over (a) CoMo/Beta, and (b) CoMo/Y.	140
Fig. 6.12. Product distribution for n-HD cracking over CoMo/Beta catalyst (Temperature - 500 °C, Pressure - 1 atm, WHSV - 83 h ⁻¹ , catalyst mass - 4 g, liquid feed injected - 3.7 g).....	141
Fig. 6.13. Composition of the gaseous product for cracking of n-HD and 1MN+n-HD over CoMo/Beta.	142
Fig. 6.14. Correlation between the selectivity towards 2-ring monoaromatics and selectivity for BTX over various catalysts for cracking of 1MN in the presence and absence of n-HD.....	143
Fig. 6.15. Conversion of 1MN for various regeneration and reuse cycles over (a) CoMo/Beta, and (b) CoMo/Y.....	144
Fig. 6.16. (a) Dependence of 1MN conversion on reaction time, and (b) Dependence of coke yield on reaction time over the CoMo/Y catalyst.	144
Fig. 6.17. Product distribution for 1MN + anthracene and 1MN + anthracene + n-HD cracking over (a) Beta zeolite and catalysts supported over Beta zeolite, (b) Y zeolite and catalysts supported over Y zeolite (Temperature - 500 °C, Pressure - 1 atm, WHSV - 83 h ⁻¹ , catalyst wt. - 4 g, liquid feed injected - 3.7 g, feed - 50 wt. % 1MN + 50 wt. % Anthracene (in the absence of n-HD) or 35 wt. % 1MN + 35 wt. % Anthracene + 30 wt. % n-HD).....	148
Fig. 6.18. Product distribution for LCO and LCO + n-HD cracking over (a) Beta zeolite and catalysts supported over Beta zeolite, (b) Y zeolite and catalysts supported over Y zeolite	

(Temperature - 500 °C, Pressure - 1 atm, WHSV - 83 h ⁻¹ , catalyst wt. - 4 g, liquid feed injected - 3.7 g, feed - LCO (in the absence of n-HD) or 70 wt. % LCO + 30 wt. % n-HD).	153
Fig. 6.19. Conversion of various diaromatics present in the LCO feed (a) in the absence of n-HD, and (b) in the presence of n-HD.	154
Fig. 6.20. Conversion of (a) lower ($\leq C_{12}$) and (b) higher ($> C_{12}$) diaromatics present in the LCO feed in the absence and presence of n-HD.	155
Fig. 6.21. Comparison of (a,b) coke yield, (c,d) BTX yield, and (e,f) MAH yield for different feeds and catalysts.	157
Fig. 6.22. Optimized structures of a) H-Beta, b) Co/Beta, c) Mo/Beta, and d) CoMo/Beta .	159
Fig. 6.23. Optimized structures of reactant (R), product (P), and transition state (TS) for the cracking of 1MN on CoMoO ₄ /Beta in the presence of H ₂ . All bond distances are in Å. Colors of atoms are represented as: grey – carbon, sea green – molybdenum, purple – cobalt, yellow – silicon, red – oxygen, magenta – aluminum, white – hydrogen.	160
Fig. 6.24. Proposed reaction pathway for cracking of (a) 1-Methylnaphthalene and (b) Anthracene.	162
Fig. 7.1. XRD pattern of Beta zeolite, CoMo(0.5)/Beta, CoMo(1)/Beta, and CoMo(2)/Beta catalysts.	167
Fig. 7.2. NH ₃ -TPD profiles of Beta zeolite, CoMo(0.5)/Beta, CoMo(1)/Beta, and CoMo(2)/Beta catalysts.	169
Fig. 7.3. H ₂ -TPR profile of Beta zeolite, CoMo(0.5)/Beta, CoMo(1)/Beta, and CoMo(2)/Beta catalysts.	173
Fig. 7.4. FE-SEM images of (a) Beta zeolite, (b) CoMo(0.5)/Beta, (c) CoMo(1)/Beta, and (d) CoMo(2)/Beta catalysts.	173
Fig. 7.5. HR-TEM images of (a) Beta zeolite, (b, e) CoMo(0.5)/Beta, (c, f) CoMo(1)/Beta, and (d, g) CoMo(2)/Beta catalysts at different resolutions.	174
Fig. 7.6. XPS spectra of Beta zeolite, CoMo(0.5)/Beta, CoMo(1)/Beta, and CoMo(2)/Beta catalysts.	175
Fig. 7.7. Raman spectra of Beta zeolite, CoMo(0.5)/Beta, CoMo(1)/Beta, and CoMo(2)/Beta catalysts.	177
Fig. 7.8. UV-DRS spectra of (a) Beta zeolite, CoMo(0.5)/Beta, CoMo(1)/Beta, and CoMo(2)/Beta catalysts.	178
Fig. 7.9. (a) 1MN conversion, (b) diaromatics conversion (c) BTX yield, and (d) coke yield over various catalysts with 1MN in the reactant mixture with and without n-HD.	179

Fig. 7.10. Correlation between BTX yield and (a) crystallite size, (b) BET surface area, (c)	180
Fig. 7.11. Correlation between (a) BTX yield and BAS/LAS ratio, (b) BTX yield and HTI, (c) BTX yield and moderate acid sites, (d) coke yield and BAS/LAS ratio, (e) coke yield and HTI, (f) coke yield and moderate acid sites.....	181
Fig. 7.12. (a) 1MN conversion, (b) ANTH conversion, (c) diaromatics conversion, (d) triaromatics conversion, (e) BTX yield, and (f) coke yield over various catalysts with 1MN + ANTH with and without n-HD.	183
Fig. 7.13. (a, b) LCO conversion, (c, d) BTX yield, (e, f) coke yield, (g, h) diaromatics conversion, and (i, j) triaromatics conversion over various catalysts with LCO in the feed with and without n-HD.	185
Fig. 7.14. Conversion of various diaromatics present in the LCO feed in the absence and presence of n-HD.	187
Fig. 7.15. LCO conversion in different experimental runs after multiple regeneration and reuse cycles over CoMo(0.5)/Beta catalyst.	187
Fig. 7.16. Effect of (a) temperature, and (b) WHSV on total MAH yield, BTX yield, coke yield, and LCO conversion for LCO + n-HD cracking on CoMo(0.5)/Beta catalyst.....	188
Fig. 7.17. (a) XRD, (b) Raman, and (c) H ₂ -TPR analysis of used CoMo(0.5)/Beta, and fresh CoMo(0.5)/Beta catalysts.	189
Fig. 7.18. Time-on-stream study for hydrocracking of (a) 1MN and (b) LCO using CoMo(0.5)/Beta catalyst.	190
Fig. 8.1. Proposed reaction network for a lumped kinetic model.	195
Fig. 8.2. Experimental and predicted model Yields for different temperatures (a) 450 °C, (b) 500 °C, (c) 550 °C, and (d) 600 °C.....	198

List of Tables

Table 1.1 Alternative Petrochemical Uses for Refinery Streams [12-17].	4
Table 2.1 Summary of products from hydroprocessing units [50,51].	17
Table 2.2 Effect of catalyst and experimental conditions on LCO hydrocracking to fuel.	23
Table 2.3 Effect of catalyst and experimental conditions in LCO Hydrocracking to BTX.	28
Table 2.4 Molecular components of various LCO samples [70].	28
Table 2.5 Summary of Kinetic Models for Catalytic Cracking.	39
Table 3.1 Various operational modes of the setup.	53
Table 4.1 Textural properties, Si/Al ratio, and acidic properties of different zeolites.	60
Table 4.2 Physicochemical characteristics and composition of the LCO sample.	61
Table 4.3 Equilibrium fraction of various diaromatics in the product for cracking of 9MA.	64
Table 4.4 Activation barrier for the interaction of BAS with the closest C-atom of 1MN.	78
Table 4.5 H-atoms for hydrogenation and degree of unsaturation of different compounds.	80
Table 5.1 Textural properties and chemical composition of zeolite-supported catalysts.	88
Table 5.2 Acidity properties of Ni and NiW catalysts.	90
Table 5.3 Acidity properties of various catalysts based on NH ₃ -TPD and Pyridine-FTIR analysis.	91
Table 5.4 Elemental composition of Ni and NiW catalysts.	94
Table 5.5 Binding energies of Ni 2p and W 4f states.	96
Table 5.6 Fraction of various diaromatics (in wt. %) in the product for cracking of 9MA over NiW/Beta catalyst in the absence and presence of n-HD.	110
Table 6.1 Textural properties of parent zeolites and Co and Mo-modified zeolite catalysts.	126
Table 6.2 Acidic properties of parent zeolites and Co and Mo-modified zeolite catalysts.	128
Table 6.3 Elemental composition of catalysts obtained by EDX.	130
Table 6.4 Binding energies of Mo 3d and Co 2p states.	132
Table 6.5 Effect of different catalysts on the cracking of 1MN in the absence of n-HD.	136
Table 6.6 Fraction of BTEX compounds in the product for cracking of 1MN in presence and absence of n-HD over various catalysts (B-benzene, T-toluene, X-xylene, EB-ethyl benzene).	136
Table 6.7 Effect of different catalysts on the cracking of 1MN in the presence of n-HD.	137
Table 6.8 Effect of different catalysts on the cracking of 1MN + anthracene in the absence of n-HD.	145

Table 6.9 Effect of different catalysts on the cracking of 1MN + anthracene in the presence of n-HD.	146
Table 6.10 Fraction of various diaromatics (in wt. %) in the product for cracking of 1MN + Anthracene over various catalysts in the absence of n-HD.	147
Table 6.11 Fraction of various diaromatics (in wt. %) in the product for cracking of 1MN + Anthracene over various catalysts in the presence of n-HD.	147
Table 6.12 Effect of different catalysts on the cracking of LCO in the absence of n-HD.....	151
Table 6.13 Effect of different catalysts on the cracking of LCO in the presence of n-HD. ..	151
Table 6.14 Activation barriers (kJ/mol) for the hydrogenation of 1MN on various catalysts in the presence of H ₂	160
Table 7.1 Textural properties of parent zeolites and Co and Mo-modified zeolite catalysts.	168
Table 7.2 Acidic properties of parent zeolites and Co and Mo-modified zeolite catalysts. ..	170
Table 7.3 Acidity properties of various catalysts based on NH ₃ -TPD and Pyridine-FTIR analysis.....	171
Table 7.4 Elemental composition of catalysts obtained by EDX.	174
Table 7.5 Binding energies of Mo 3d and Co 2p states.	175
Table 7.6 Comparative Table of Current Work and Relevant Studies.	191
Table 8.1 Optimized kinetic parameters along with confidence intervals for lumped kinetic modelling.	198